

Transport and dynamical properties for a bouncing ball model with regular and stochastic perturbations

^{1,2,3}Diogo Ricardo da Costa, ²Carl P. Dettmann and ³Edson D. Leonel

¹*Instituto de Física da USP, Rua do Matão, Travessa R,*

187 - Cidade Universitária - 05314-970 - São Paulo - SP - Brazil

²*School of Mathematics, University of Bristol, Bristol, United Kingdom*

³*Departamento de Física, UNESP - Univ Estadual Paulista,*

Av.24A, 1515 - 13506-900 - Rio Claro - SP - Brazil

(Dated: June 27, 2014)

Some statistical properties related to the diffusion in energy for an ensemble of classical particles in a bouncing ball model are studied. The particles are confined to bounce between two rigid walls. One of them is fixed while the other oscillates. The dynamics is described by a two dimensional nonlinear map for the velocity of the particle and time at the instant of the collision. Two different types of change of momentum are considered: (i) periodic due to a sine function and; (ii) stochastic. For elastic collisions case (i) leads to finite diffusion in energy while (ii) produces unlimited diffusion. On the other hand, inelastic collisions yield either (i) and (ii) to have limited diffusion. Scaling arguments are used to investigate some properties of the transport coefficient in the chaotic low energy region. Scaling exponents are also obtained for both conservative and dissipative case for cases (i) and (ii). We show that the parameter space has complicated structures either in Lyapunov as well as period coordinates. When stochasticity is introduced in the dynamics, we observed the destruction of the parameter space structures.

PACS numbers: 05.45.-a, 05.45.Pq, 05.45.Tp

I. INTRODUCTION

Unlimited diffusion in energy of a classical particle due to collisions with an infinitely heavy and moving wall was called as Fermi acceleration [1]. The original idea was proposed by Enrico Fermi in 1949 as an attempt to explain a possible origin of the high energy of the cosmic rays. Fermi claimed that the unlimited diffusion in energy (which leads to the Fermi acceleration phenomena) was due to interactions of the charged particles with the time varying magnetic fields present in the space. After his original idea was launched, several systems were proposed in the literature trying to model and describe the unlimited diffusion [2–14]. Among several models, one that we discuss in this paper is often called the Fermi-Ulam model (FUM). It consists of a classical particle, or then an ensemble of non interacting particles, confined to move between two rigid walls [15–27]. One of them is moving in time therefore corresponding to the time-varying magnetic fields and the other one is fixed. The functionality of the second one is just to produce a returning mechanism for a further collision with the moving wall.

A modification of the Fermi-Ulam model was suggested some years ago, it was called as the bouncer ball model [28, 29]. It considers a particle falling down, in a constant gravitational field, on a moving platform. Different approaches to the bouncer model have been studied theoretically and experimentally [8, 30–32]. One example can be cited, which considers a propagating surface wave that travels on the surface of the platform, while the platform remains motionless [32]. This model can be used to describe the transport of particles by propagating surface

waves, which is an important problem with numerous applications including powder transport by piezoelectrically excited ultrasonic surface wave [33] and manipulation of bioparticles using traveling wave electrophoresis [32, 34].

For a sufficiently smooth and periodic movement of the moving wall in the FUM, the dynamics of the particle leads to three different types of behaviour (see for instance [9]): (i) regular - characterized by period motion; (ii) quasi-periodic - leading the invariant spanning curves or even curves circling periodic fixed points and; (iii) chaotic dynamics yielding in an unpredictability of the dynamics. The dynamics is often described by a two dimensional, nonlinear and area preserving mapping for the variables velocity of the particle and instant of the collisions with the moving wall. The chaotic sea is not allowed to diffuse with unbounded energy due to the existence of a set of infinitely many invariant spanning curves in the phase space [9]. Indeed, the position of the lowest one defines the law of the behaviour of several observables along the chaotic sea, including average velocity [16], deviation around the average velocity and many others. It is then concluded from the literature that a periodic perturbation of the moving wall leads to a failure to generate unlimited diffusion. This is basically connected to the fact the high energy of a bouncing particle leads to correlation between two successive collisions therefore producing regularity in the dynamics. For stochastic perturbation of the moving wall, the energy of the particle undergoes unlimited diffusion. Such diffusion is however limited when a fractional loss of energy is introduced upon collision with the moving wall [10] via introduction of a restitution coefficient. Other types of dissipation also prevent the unlimited diffusion including

a viscous drag force [35, 36].

In this paper we revisit the Fermi-Ulam model seeking to understand and describe some of its dynamical properties considering three regimes of external perturbation: (i) entirely stochastic; (ii) totally periodic and; (iii) low stochasticity. For case (i) we confirm the unlimited diffusion in energy is taking place for elastic collisions but is suppressed when a fractional loss of energy upon collisions is introduced. Then we explore some properties around the steady state particularly focusing on the characterization of the diffusion coefficient. Our results show it is indeed scaling invariant with respect either to the number of collisions as well as the restitution coefficient. For case (ii) we discuss some of the dynamical properties present in the parameter space of the model including the so called shrimp-like structures obtained as a function of the Lyapunov exponent as well as the period. Finally for case (iii) we explore the influences of the stochasticity in the periodic structures present in the parameter space and how they change as the stochastic parameter rises.

The organization of this paper is as follows. In Sec. II we discuss the model and the map. Section III is devoted to discuss the stochastic model focusing particularly on the diffusion coefficient and its scaling invariance. The deterministic model and parameter space is left for Sec. IV while the influences of a partially stochastic dynamics is discussed in Sec. V. Conclusions and final remarks are presented in Sec. VI.

II. THE MODEL AND THE MAP

The model we consider in this paper is a simplified version of the Fermi-Ulam model [9]. It consists of a classical particle - or an ensemble of non-interacting particles - confined to bounce between two rigid walls. Because of the simplification both walls are assumed to be fixed. However when the particle collides with one of them, say the one in the left, it suffers an exchange of energy and momentum due to the collision as if the wall were moving. The other wall is introduced as a returning mechanism for the particle to collide again with the wall responsible for the exchange of energy. This simplification was very convenient in earlier years to speed up numerical simulations when computers were far slower. Such version is still very useful nowadays because it facilitates the analytical treatment enormously. It also retains many properties of the complete model in the limit of high energy and smaller oscillations. Two types of exchange of energy are considered: (i) smooth due to a sine periodic function and; (ii) abrupt due to an uncorrelated random function. The dynamics of the particle is given by a two dimensional nonlinear map for the velocity of the particle and time immediately after the collision with the wall. Considering dimensionless variables (see [10]), the mapping that describes the dynamics of the particle is written as

$$T : \begin{cases} \phi_{n+1} = [\phi_n + \frac{2}{v_n} + 2\pi\delta Z] \text{ mod}(2\pi) \\ v_{n+1} = |\alpha v_n - (1 + \alpha)\epsilon \sin(\phi_{n+1})| \end{cases}, \quad (1)$$

where $\alpha \in [0, 1]$ denotes the restitution coefficient, $\epsilon \in [0, 1]$ corresponds to amplitude of the maximum velocity of the *moving wall* and $\delta \in [0, 1]$ corresponds to the strength of the stochastic perturbation. Let us discuss more on the stochastic perturbation. Indeed in a real experiment, the position of the moving wall is given by an external engine with limited power. Of course the stochastic perturbation could be interpreted as due to imperfections of the system. As for example the engine suffering influences of external noise, like electric fluctuations, therefore causing disturbs to the motion of the moving wall. Additionally, one may think the particle, which in an experiment could be a sphere, has also imperfections in the shape. Most likely such imperfections could lead the particle to rotate, transferring translational energy to rotational. All of these terms can be modelled by a stochastic perturbations. For $\alpha = 1$ there is no dissipation and collisions are elastic. For the case of $\alpha < 1$ the particle experiences a fractional loss of energy upon collision. The parameter ϵ is responsible for controlling the non-linearity of the system. For $\epsilon = 0$ and considering the conservative case and deterministic dynamics, the system is integrable because the energy is a constant of motion. Therefore only periodic and quasi-periodic motion is observed in the phase space. On the other hand for $\epsilon \neq 0$ the system is non integrable and chaos may be observed in the dynamics. Then ϵ plays an important role in the dynamics particularly controlling a transition from integrability to non-integrability. The parameter δ determines a transition from deterministic for $\delta = 0$ to stochastic dynamics when $\delta \neq 0$. The term $Z \in [0, 1]$ is a uniform random number obtained by using a generator RAN2 in Fortran code and can be found in numerical recipes libraries [37]. Because we are using a simplified version, the modulus function used in second equation of mapping (1) is introduced to avoid the particle having negative velocity after a collision with the wall in the left. In the complete version, negative velocities are allowed and indeed observed. However in the simplified version they are forbidden and can be interpreted as the particle moving beyond the walls. In such a situation, the modulus function is used just to re-inject the particle back to the inner region of the walls with the same velocity.

The possible types of motion of the particle depend on the combination of α , ϵ and δ . Let us start with $\delta = 0$ leading the dynamics to be deterministic. Then two possibilities arise for $\epsilon = 0$: (i) for $\alpha = 1$ the system is integrable due to the energy preservation. Only periodic and quasi-periodic dynamics are observed in the phase space. (ii) For $\alpha \neq 1$, the particle has a fractional loss of energy and stationary state is given by the null energy leading the particle to reach the state of rest. The decay of velocity is given by $v_n = \alpha^n v_0$ where v_0 is the initial velocity. For $\epsilon \neq 0$, the integrability is destroyed and again two possibilities arise: (i) for $\alpha = 1$, the phase space is mixed and exhibits a set of periodic islands surrounded by a chaotic sea that is limited by a

set of infinite invariant spanning curves. They prevent the particle to diffuse to unbounded velocities then suppressing Fermi acceleration. The chaotic sea scales with the control parameter ϵ leading to several observables of the phase space to be scaling invariant with respect to ϵ . The scenario changes substantially for $\alpha \neq 0$ then; (ii) the mixed structure of the phase space is entirely destroyed by the presence of dissipation. Elliptic fixed points may turn into sinks and depending on the basin of attraction may lead the asymptotic dynamics to be attracted to the sinks and stay there forever characterizing then a steady state. The invariant spanning curves are all destroyed and for $\alpha \cong 1$ but still less than 1, multiple periodic attractors are observed [38, 39] while for large dissipation, typically $\alpha < 0.5$, boundary crisis can be characterized as well as route to chaos via period doubling is often observed [40]. At the regime of strong dissipation, periodic structures in the phase space called *shrimps* [41–43] can be observed too [44]. For $\delta \neq 0$ the stochastic dynamics dominates. Of course for $\epsilon = 0$ nothing happens then let us pose the possibilities for $\epsilon \neq 0$. The first case is $\alpha = 1$ i.e., the non dissipative case. The mixed structure is again destroyed, particularly the invariant spanning curves. However due to the fact the variable ϕ is now random, the sine function also becomes random leading to a diffusion in the velocity. On the other hand for $\alpha < 1$ the unlimited diffusion is suppressed leading the dynamics of the particle to be confined in a finite region of the phase space. Such confinement can be described by using scaling formalism. In what follows we discuss the different situations namely, $\delta = 1$, $\delta = 0$ and $0 < \delta < 1$.

III. RESULTS FOR $\delta = 1$

In this section we discuss the completely stochastic case $\delta = 1$. As discussed above, for $\alpha = 1$ unlimited diffusion in velocity should be observed. Results for different values of δ shall be shown later in the paper.

Considering the second equation of the map (1), we can show after an ensemble average that

$$\overline{v_{n+1}^2} = \alpha^2 \overline{v_n^2} + \frac{(1+\alpha)^2}{2} \epsilon^2, \quad (2)$$

where $\overline{v^2}$ corresponds to the average of v^2 .

In the conservative case $\alpha = 1$ the average (RMS) velocity grows with an exponent 1 with respect to ϵ and 1/2 with respect to n :

$$v_{rms} = \sqrt{\overline{v^2}} = \sqrt{v_0^2 + 2\epsilon^2 n}, \quad (3)$$

for large n , or small v_0 . This scaling was previously discussed in [10].

The analytical finding is confirmed by numerical simulations, as shown in Fig. 1 for different values of ϵ . The simulations were made as follows. First we set an initial velocity $v_0 = \epsilon$. Then we evolved an ensemble of

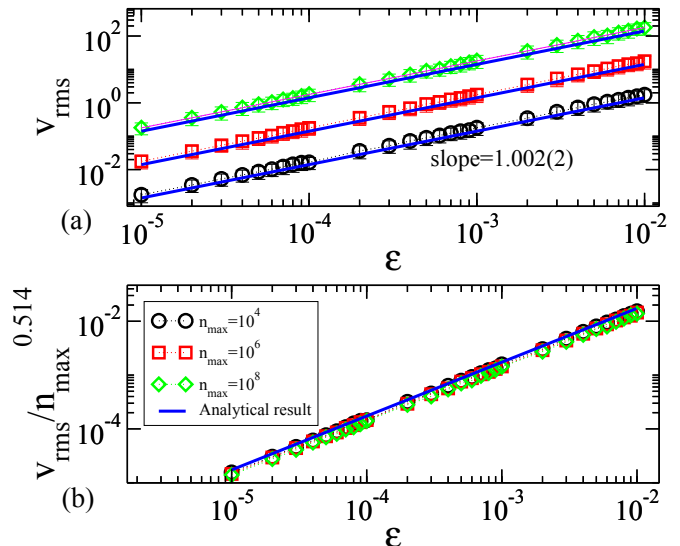


FIG. 1: (Colour online) Plot of: (a) v_{rms} as a function of ϵ for three different values of the maximum number of iterations n_{max} namely ($n_{max} = 10^4$, $n_{max} = 10^6$ and $n_{max} = 10^8$). (b) Rescale of the vertical axis for the curves shown in (a) after the transformation $\bar{v} \rightarrow \bar{v}/n_{max}^{0.514}$. The analytical results are shown as blue straight lines.

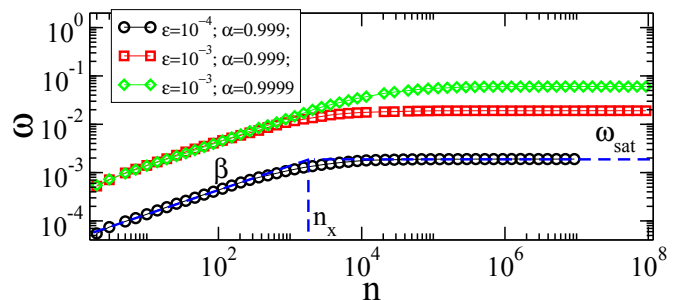


FIG. 2: (Colour online) Plot of ω vs n for three different values of ϵ and α . The slope of growth is $\beta \cong 0.5$ obtained after a power law fit. The saturation and crossover are indicated in the figure.

500 different initial phases $\phi_0 \in [0, 2\pi]$ calculating the velocity $v_{rms} = \sum_{j=1}^{500} v_n(j)/500$ at different number of collisions, denoted as n_{max} and considering different values of the parameter ϵ , as shown in Fig. 1(a). After doing a power law fitting we obtained that all curves have slope approximately 1, as shown in the figure and confirming the analytical finding. As one sees the greater n_{max} the greater v_{rms} maximum is obtained for a particular value of ϵ . The behaviour of v_{rms} confirms previous result obtained in Ref. [10] since for $\epsilon = 10^{-5}$ we obtained $v_{rms} \cong n^{0.514(1)}$. Using this result to rescale the vertical axis of Fig 1(a), i.e. doing $v_{rms} \rightarrow v_{rms}/n_{max}^{0.514}$, we show all curves generated for different values of n_{max} overlap each other onto a single and universal plot, as expected. Figure 1(b) shows such overlap of curves. The blue straight lines in Figs. 1(a,b) were obtained using

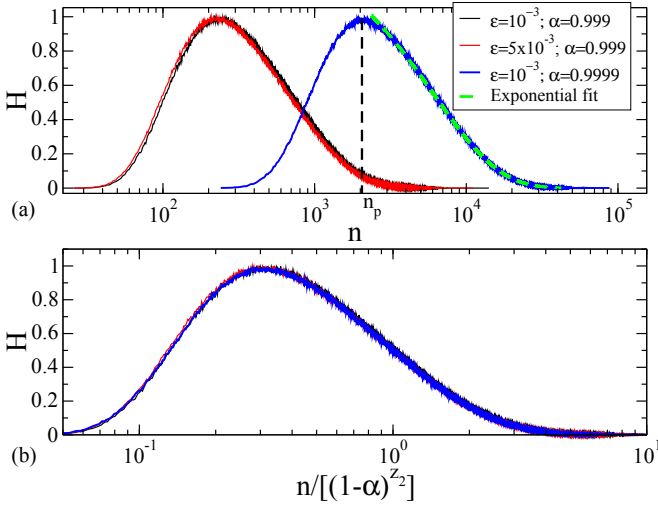


FIG. 3: (Colour online) Plot of: (a) histogram of frequency for the number of particles that have reached h as a function of the number of collisions n for different control parameters. (b) Overlap of (a) onto a single and universal plot after a rescaling of the horizontal axis.

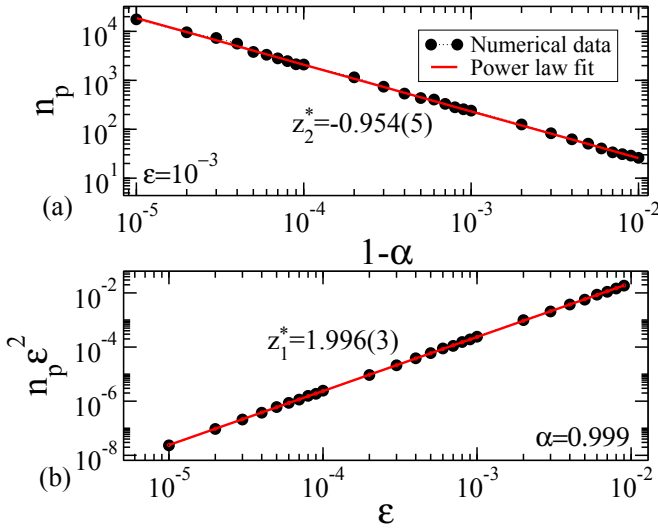


FIG. 4: (Colour online) Plot of: (a) n_p vs $(1-\alpha)$ for $\epsilon = 10^{-3}$; (b) $n_p \epsilon^2$ vs ϵ using $\alpha = 0.999$.

Eq. (3). As one can see the numerical result fits well with the analytical prediction.

Now we consider the case of $\alpha < 1$. Subtracting $\overline{v_n^2}$ in both sides of the Eq. (2) we have

$$\overline{v_{n+1}^2} - \overline{v_n^2} = \frac{\overline{v_{n+1}^2} - \overline{v_n^2}}{(n+1) - n} = \frac{(1+\alpha)^2}{2} \epsilon^2 + \overline{v_n^2} (\alpha^2 - 1), \quad (4)$$

where

$$\frac{\overline{v_{n+1}^2} - \overline{v_n^2}}{(n+1) - n} \cong \frac{d\overline{v^2}}{dn}. \quad (5)$$

We now rearrange the terms in this equation and con-

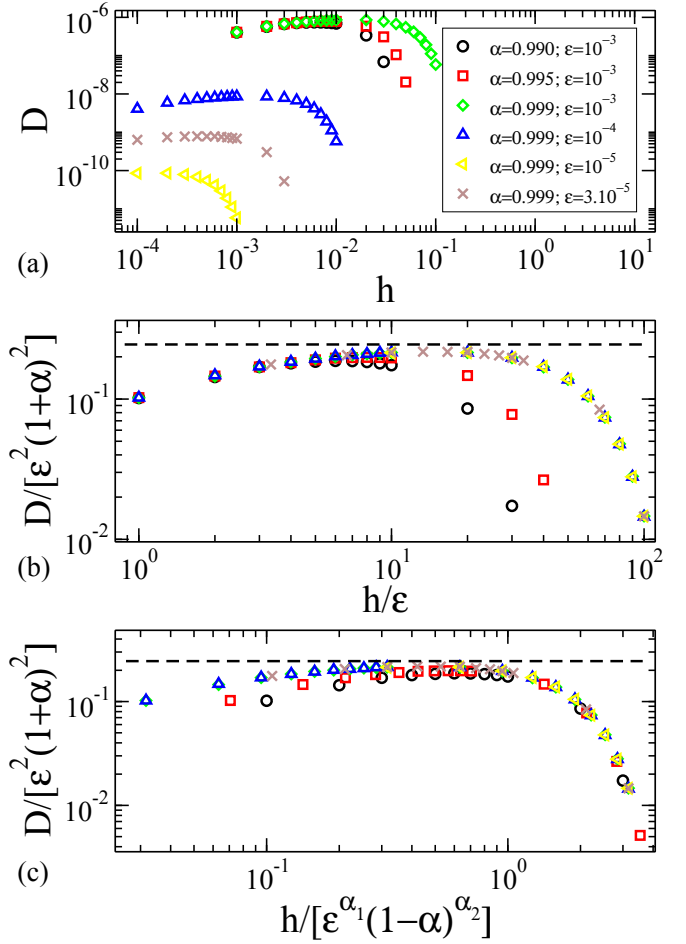


FIG. 5: (Colour online) Plot of: (a) D vs h for different values of α and ϵ ; (b) overlap for all curves presented in (a) after a rescaling of the axis for low values of h ; (c) overlap of all curves presented in the item (a) after a proper rescale in the axis for high values of h .

sider $\overline{v^2} = E$, which implies that $d\overline{v^2} = dE$, as result we obtained

$$\frac{dE}{E(\alpha^2 - 1) + \frac{(1+\alpha)^2}{2} \epsilon^2} = dn. \quad (6)$$

Considering $u = E(\alpha^2 - 1) + \frac{(1+\alpha)^2}{2} \epsilon^2$ and $du = dE(\alpha^2 - 1)$ yields

$$\int_{u_0}^u \frac{du}{u} = (\alpha^2 - 1) \int_0^n dn. \quad (7)$$

Therewith we find

$$u = u_0 e^{(\alpha^2 - 1)n}. \quad (8)$$

Returning to the variable $\overline{v^2}$ we obtain

$$\overline{v^2} = \frac{\epsilon^2}{2} \left(\frac{1+\alpha}{1-\alpha} \right) \left[1 - e^{(\alpha^2 - 1)n} \right] + v_0^2 e^{(\alpha^2 - 1)n}. \quad (9)$$

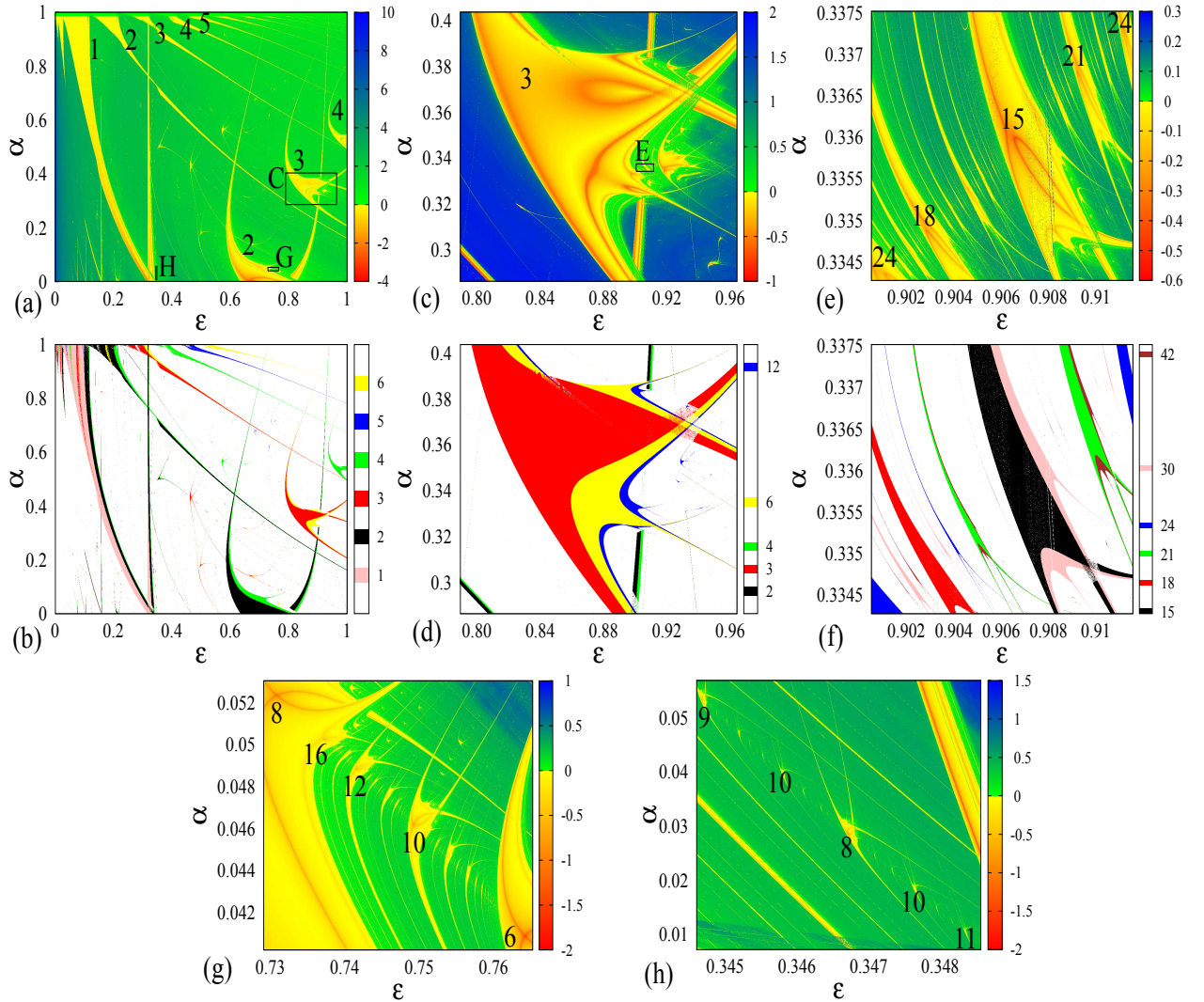


FIG. 6: (Colour online) Parameter space for $\delta = 0$ considering a grid of $10^3 \times 10^3$ cells. For (a), (c), (e), (g) and (h) we present the maximum Lyapunov exponent, where the exponents were coded with a continuous colour scale ranging from red-yellow (negative exponents) to green-blue (positive exponents). For (b), (d) and (f) the colours represent the period. We have considered fixed initial conditions of $v_0 = 0.1$ and $\phi_0 = 6$.

For $n \rightarrow \infty$ we find

$$v_{rms} = v_{sat} = \sqrt{(1+\alpha)/2}(1-\alpha)^{-1/2}\epsilon. \quad (10)$$

In terms of the scaling discussed in Ref. [10], $\bar{v}_{sat} \propto \epsilon^{\alpha_1}(1-\alpha)^{\alpha_2}$ we thus have $\alpha_1 = 1$ and $\alpha_2 = -0.5$.

Considering small values of v_0 in the Eq. (3) and equating to Eq. (10), we find the crossover n_x given by the following equation

$$n_x = \left(\frac{1+\alpha}{4}\right)(1-\alpha)^{-1}. \quad (11)$$

The crossover n_x scales as $(1-\alpha)^{-1}$ independent of ϵ . In terms of the scaling discussed in Ref. [10], $n_x \epsilon^2 \propto \epsilon^{z_1}(1-\alpha)^{z_2}$ we thus have $z_1 = 2$ and $z_2 = -1$.

The RMS velocity gives only a single measure of the distribution. We propose that the above exponents apply more generally, and test this by considering the deviation around of the average velocity defined as

$$\omega(n, \epsilon, \alpha) = \frac{1}{M} \sum_{k=1}^M \sqrt{v_k^2(n, \epsilon, \alpha) - \bar{v}^2(n, \epsilon, \alpha)}. \quad (12)$$

Here M denotes an ensemble of different initial conditions. Figure 2 shows three curves of ω for different values of α and ϵ . Our simulations were made considering an ensemble of $M = 500$ different initial conditions. Starting the ensemble with $v_0 = \epsilon$ and varying $\phi_0 \in [0, 2\pi]$, one sees that for short n all curves grow to start with a slope of $\beta \cong 0.5$. After a crossover n_x they

bend towards a regime of saturation (ω_{sat}). After doing the corresponding simulations we obtain $\alpha_1 = 1.0011(2)$, $\alpha_2 = -0.5002(1)$, $z_1 = 2.001(2)$ and $z_2 = -1.018(2)$, in good agreement with those above and obtained in Ref. [10].

For a further test, and to lead onto the discussions for the case of $\delta = 1$ we concentrate now on some transport properties along the phase space. Specifically, we consider the number of collisions given by a particle over the chaotic region until reaching a certain velocity h in the phase space [45]. We define h as a fraction of v_{rms} given by Eq. (3). To run the simulations we considered a large ensemble of 10^7 different initial conditions with $v_0 = \epsilon$ and different $\phi_0 \in [0, 2\pi)$ randomly chosen. If along the dynamics the velocity of the particle is larger or equal to h , we collect the number of iterations n until that time and a new initial condition is started. A histogram of frequency for the number of particles that reach h in a time n is shown in Fig. 3(a). The vertical axis was rescaled to 1 for visual purposes.

When we look at the histograms we see that for small n the number of particles that reach h is practically zero. It rises to a maximum when the number of collisions is n_p . After this point, the histogram has a behaviour marked by an exponential decay. In Fig. 4(a) we have the corresponding values of n_p for the histogram as a function of $(1 - \alpha)$. The slope obtained is equal to $z_2^* = -0.954(5)$. We emphasize this slope is quite close to the numerical value obtained for z_2 and previously obtained in [10] for n_x vs $(1 - \alpha)$, i.e. $z_2 = -1.018(2)$. Varying then the parameter ϵ , we obtained $z_1^* = 1.996(3)$ as shown in Fig. 4(b). Using the results obtained for the histogram of frequency we can rescale the horizontal axis of Fig. 3(a) by doing a transformation of the type $n \rightarrow n\epsilon^2/[\epsilon^{z_1^*}(1 - \alpha)^{z_2^*}]$. The result is shown in Fig. 3(b) and confirms a scaling invariance of the histogram of frequency with respect of α .

The result obtained from the histogram of frequency can be extended to study the diffusion coefficient D . Indeed if we proceed similarly as made recently in Ref. [46] we end up with a decay of the histogram after reaching the peak at n_p described by $H \propto \exp[-Dn\pi^2/h^2]$. Here D is the diffusion coefficient. Indeed D can be written as $D = 4h^2\mu/\pi^2$, where $\mu = (1 - \alpha)^{z_2}$.

Figure 5(a) shows a plot of D vs h for different values of α and ϵ . We see that D is almost constant for a large range of h for different α and ϵ . However when h reaches the region around the stationary state given by $(1 + \alpha)\epsilon/\sqrt{2}$ it suffers a marked decrease. Because $\alpha < 1$ the particle has a limited region to visit then this decrease is expected since the velocity of the particle can not diffuse unlimited.

Different rescales can be considered for the characterization of D . For low values of h the vertical axis of Fig. 5(a) can be rescaled as $D \rightarrow D/[\epsilon^2(1 + \alpha)^2]$ while the horizontal axis is transformed by $h \rightarrow h/\epsilon$. The results are shown in Fig. 5(b). For high values of h the rescale in the vertical axis is the same, but in the horizontal axis

is done by $h \rightarrow h/[\epsilon^{\alpha_1}(1 - \alpha)^{\alpha_2}]$. Indeed if we consider the mapping (1) for $\alpha < 1$ and the expression obtained in the Eq. (2) we can write that

$$\overline{v_{n+1}^2} - \overline{v_n^2} = \langle \Delta^2 \rangle = \overline{v_n^2}(\alpha^2 - 1) + \frac{(1 + \alpha)^2}{2}\epsilon^2.$$

In the limit of $\alpha \cong 1$ but still less than 1, the diffusion coefficient is then given by $D \cong \langle \Delta^2 \rangle/2$. We conclude in the limit of $\alpha \cong 1$ that $D/[(1 + \alpha)^2\epsilon^2] \cong 1/4$ for the initial velocity $v_0 \rightarrow 0$. The limit $D = 1/4$ is shown in Figs. 5(b,c) as dashed lines.

IV. PARAMETER SPACE FOR $\delta = 0$

In this section we discuss the case $\delta = 0$, i.e., the deterministic case. Two possible situations can be discussed for $\epsilon \neq 0$, which include: (i) $\alpha = 1$ leading to the non-dissipative case and; (ii) $\alpha < 1$ yielding in a dissipative dynamics. For the conservative case the phase space is mixed exhibiting a set of periodic islands surrounded by low energy chaotic sea limited by an infinite set of invariant spanning curves[9]. The situation for $\alpha < 1$ is

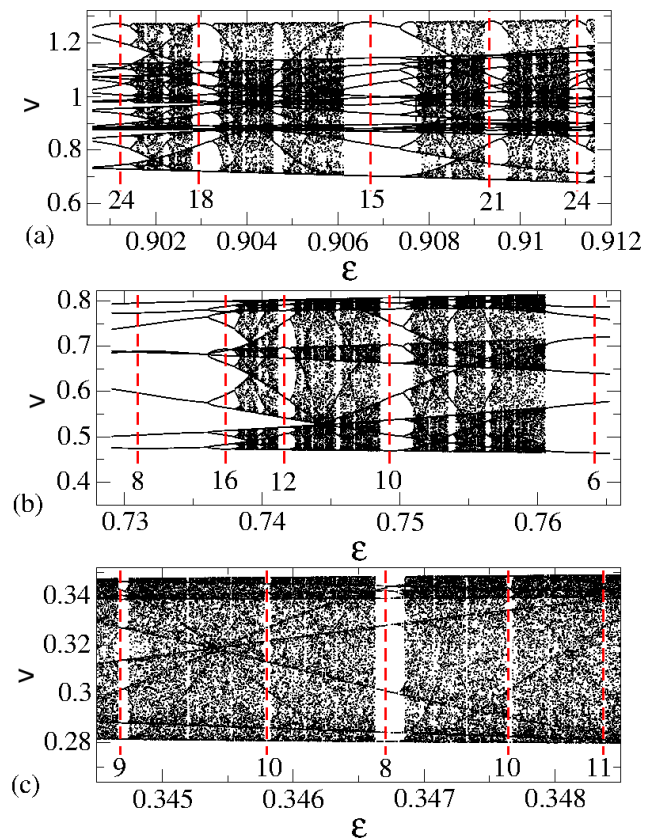


FIG. 7: (Colour online) Plot of a bifurcation diagram for the variable velocity as function of ϵ where α is given by the following expressions: (a) Eq. (14); (b) Eq. (15); (c) Eq. (16). We have considered fixed initial conditions of $v_0 = 0.1$ and $\phi_0 = 6$.

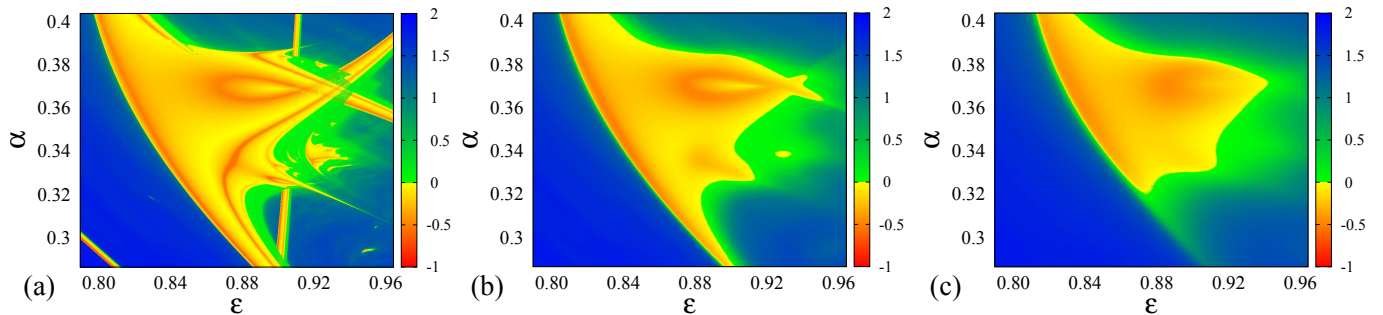


FIG. 8: (Colour online) Plot of the parameter space coloured by the Lyapunov exponent considering the same range of parameters as shown in Fig. 6(c). We considered different values of δ : (a) $\delta = 0.00484$; (b) $\delta = 0.00024$; (c) $\delta = 0.01$.

remarkably different in the sense attractors are present in the dynamics [35, 38, 39]. Our goal in this section is to investigate the dynamics of the particle looking at the parameter space α vs ϵ . Figure 6(a) shows a plot of α vs ϵ where the colour scheme represents the maximum Lyapunov exponent. The degrade of red to yellow denotes regular dynamics marked by periodic behaviour. Green to blue characterize chaos. As well known in the literature [47], the Lyapunov exponent is extensively used to characterize unpredictability in nonlinear systems. They can be obtained from

$$\lambda_j = \lim_{n \rightarrow \infty} \frac{1}{n} \ln |\Lambda_j^{(n)}|, \quad j = 1, 2 \quad (13)$$

where $\Lambda_j^{(n)}$ are the eigenvalues of the matrix $\tilde{M} = \prod_i^n J_i(v_i, \phi_i)$ and J_i is the Jacobian matrix evaluated along the orbit (v_i, ϕ_i) . If at least one of the λ_j is positive, then the system is said to have chaotic components.

The procedure used to construct Fig. 6(a) was to divide both axis of $\epsilon \in [0.0001, 1]$ and $\alpha \in [0, 1]$ into windows of 1000 parts each. This leads to a plot of a fine grid containing 10^6 different cells in the parameter space. For each cell we consider an initial condition and evolve it in time for a very long run. For all simulations of parameter space we have considered a fixed initial condition of $v_0 = 0.1$ and $\phi_0 = 6$. We considered a transient of 10^5 collisions of the particle with the wall and the Lyapunov exponent was computed after this transient for a total of next 10^5 collisions. The exponents were coded with a continuous colour scale ranging from red-yellow (negative exponents - regular dynamics) to green-blue (positive exponents - chaotic dynamics), as one can see in Fig. 6(a). The period of the regular regions in the parameter space of Fig. 6(a) is written in the figure. The left upper part of the figure has periodic regions with period 1, 2, 3, ... The lower part of the figure shows a chain of periodic regions with period 2, 3, 4. Figure 6(b) shows the parameter space however instead of consider the Lyapunov exponent to define the colour scheme we used the period. For period larger than 6 we painted as white colour. Figures 6(c,d) show a magnification of the region C in Fig. 6(a) where the colour represents the maximum Lyapunov exponent and the period, respectively. As expected, we see a remarkably reproduction

of the structures either considering the Lyapunov exponent or period. As observed in Fig. 6(d) we have a large region with period 3 followed by a duplication of period as marked by yellow colour with period 6. Furthermore a second duplication of period occurs as observed in the blue region with period 12. Figures 6(e,f) show another magnification but now in the region E of Fig. 6(c). We see there are sequences of period that are multiple of 3 (for example, we highlighted the periods 15, 18, 21 and 24). It happens because the structures tend to follow the period of the larger period 3 region shown in Fig. 6(c). Similar behaviour happens for the period 2 region shown in the lower part of Fig. 6(a). Figure 6(g) shows an enlargement of box G in Fig. 6(a) where periods found here are multiple of 2 leading to 6, 8, 10, 12 and 16. Finally Fig. 6(h) shows a magnification of the H box in Fig. 6(a) where we see that periods here are multiple of 1 leading to 8, 9, 10 and 11.

The periodic regions represented in Figs. 6(e,g,h) can be described by using a linear equation in the parameter space. Therefore the position of the periodic regions are given by: (i) for Fig. 6(e)

$$\alpha(\epsilon) = 0.069(2) + 0.295(3)\epsilon; \quad (14)$$

(ii) for Fig. 6(g)

$$\alpha(\epsilon) = 0.305(3) + 0.346(4)\epsilon; \quad (15)$$

and finally (iii) for Fig. 6(h)

$$\alpha(\epsilon) = 4.09(5) + 11.7(1)\epsilon. \quad (16)$$

Considering the organization of the periodic regions are described by the three equations above, we can use such relations to obtain the bifurcation diagrams for the variable velocity as a function of ϵ , as shown in Figs. 7(a,b,c) and using respectively Eqs. (14), (15) and (16).

V. RESULTS FOR $0 < \delta < 1$

In this section we discuss the case of $0 < \delta < 1$. The results obtained in previous sections include $\delta = 1$ and $\delta = 0$. The influences of different values of δ in some

dynamical variables are discussed now. Figures 8(a,b,c) show plots of parameter space coloured by Lyapunov exponent. Each plot was constructed by using different values of δ namely: (a) $\delta = 0.00484$; (b) $\delta = 0.0024$ and; (c) $\delta = 0.01$. As one can see for $\delta = 0.00484$ some smaller and thinner periodic regions are destroyed. After increasing a little bit more the control parameter δ , for example, for $\delta = 0.0024$ or $\delta = 0.01$, the large period 3 region is basically the only one that still remains visible and survive the perturbation. It happens because such region has a basin of attraction greater than the other periods larger than 3. Increasing the value of δ leads to increase the perturbation of ϕ in the first equation of the mapping (1). This makes easier the orbit to leave a sink region and its corresponding basin of attraction. For $\delta \rightarrow 1$ the periodic regions are no longer visible. Depending on the value of δ one can study how hard is to an orbit to leave the vicinity of a sink. It can be done observing the behaviour of ω for different values of δ , as shown in Fig. 9. As we can see for $\delta = 1$ the deviation of the average velocity is described by a power law showing a growth with slope approximately 1/2. For $\delta < 1$ we see the curves exhibit an intermittent behaviour before start growing unbounded with slope 1/2. If $\delta \rightarrow 0$ the curve of ω approaches a saturation and unlimited diffusion in velocity is no longer observed. The intermittent behaviour mentioned is due to the time in which an orbit gets stuck near the vicinity of a sink.

Let us now obtain the behaviour of the average velocity \bar{v} along an ensemble using a variation of ϵ for fixed values of δ and considering the conservative case of $\alpha = 1$. \bar{v} is defined as $\bar{v} = \frac{1}{n} \sum_{i=1}^n \frac{1}{M} \sum_{j=1}^M v_{ij}$. The curves of average velocity are obtained for an ensemble of $M = 500$ different initial conditions with $v_0 = \epsilon$ and $\phi_0 \in [0, 2\pi)$ randomly chosen. We calculate the average velocity \bar{v} as a function of n as shown in Fig. 10(a), for $\delta = 0.006$.

To prove a scaling invariance of the curves we have considered a straight line with $\bar{v} = 5.7841$ (other values lead to similar results) and we calculated the number of collisions n that intercept with the different curves. As a result we obtained that the slope after a power law fit is equal to $-2.06(1) \cong -2$. Therefore it is possible to rescale properly the horizontal axis of the Fig. 10(a)

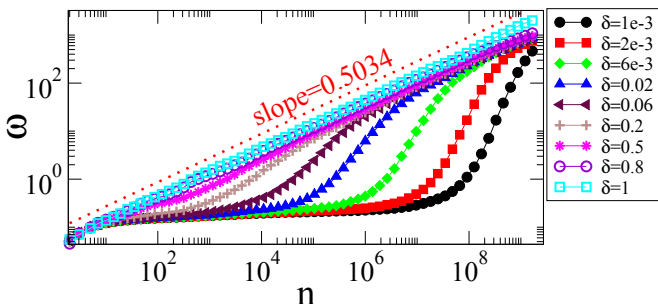


FIG. 9: (Colour online) Plot of ω vs n considering different values of δ .

considering $n \rightarrow n/\epsilon^{-2}$ (see Fig. 10(b)). Figures 10(a,b) were obtained for the parameter $\delta = 0.006$. We considered a larger value of $\delta = 0.1$ to obtain Figs. 10(c,d) while Figs. 10(e,f) were constructed for $\delta = 0.5$. The transformation $n \rightarrow n/\epsilon^{-2}$ is applied to Figs. 10(b,d,f) and a better overlap of the curves are observed for a larger δ , as shown in Fig. 10(f).

VI. SUMMARY AND CONCLUSIONS

As a short summary, we studied some dynamical properties of an ensemble of classical particles confined to bounce between rigid walls. The model is described by a two dimensional and nonlinear mapping for the variables velocity of the particle and time at the instant of the collision. We considered the dynamics for periodic and stochastic oscillations. The first leads to limited diffusion for conservative dynamics while the second produces unlimited diffusion (Fermi acceleration). When in-

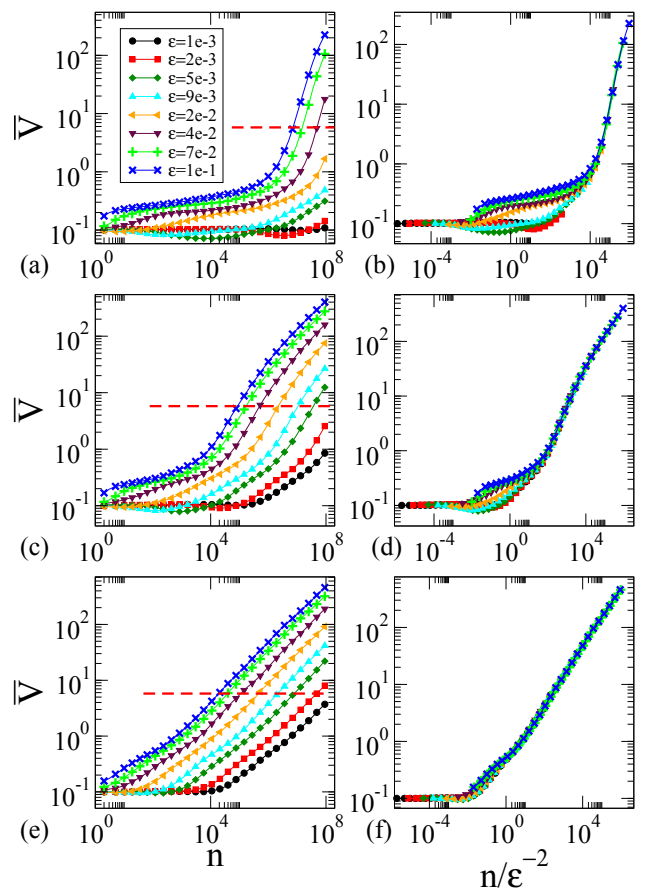


FIG. 10: (Colour online) Plot of \bar{v} vs n for different values of ϵ and considering: (a) $\delta = 0.006$; (c) $\delta = 0.1$; (d) $\delta = 0.5$. In (b), (d) and (f) we have the same curves shown in (a), (c) and (e) but now a rescale in the horizontal axis was applied ($n \rightarrow n/\epsilon^{-2}$). For all curves we have considered $\alpha = 1$ and an ensemble of 500 different initial conditions were chosen with $v_0 = \epsilon$ and $\phi_0 \in (0, 2\pi]$.

elastic collisions were introduced, unlimited diffusion of the energy was suppressed. We have used scaling arguments to investigate the system, and scaling exponents were obtained for both dissipative and conservative cases. We have shown the diffusion coefficient is scaling invariant with respect to the control parameters as well as the number of collisions. The parameter space has complicated structures present either in Lyapunov as well as period coordinates. When stochasticity is introduced in the dynamics, we observed that some periodic regions in the parameter space are destroyed. In this sense, some orbits which are in the vicinity of a sink can escape from this region. It influences the behaviour of the deviation of

the average velocity, and can delay the diffusion process.

VII. ACKNOWLEDGEMENTS

DRC acknowledges Brazilian agency FAPESP (2010/52709-5, 2012/18962-0 and 2013/22764-2). EDL thanks to CNPq, FUNDUNESP and FAPESP (2012/23688-5), Brazilian agencies. This research was supported by resources supplied by the Center for Scientific Computing (NCC/GridUNESP) of the São Paulo State University (UNESP).

-
- [1] E. Fermi, *Phys. Rev.* **75**, 1169 (1949).
- [2] S. Ulam, in *Proceedings of the Fourth Berkeley Symposium on Mathematical Statistics and Probability*, edited by J. Neyman, University of California Press, Berkeley, 1961, Vol. 3, p. 315.
- [3] R. M. Everson, *Physica D* **19**, 355 (1986).
- [4] P. J. Holmes, *J. Sound and Vibr.* **84**, 173 (1982).
- [5] A. D. Pustynnikov, *Mat. Sb.* **185**, 113 (1994). Translation in *Russian Acad. Sci. Sb. Math.* **82**, 231 (1995).
- [6] G. A. Luna-Acosta, *Phys. Rev. A* **42**, 7155 (1990).
- [7] A. J. Lichtenberg, M. A. Lieberman, *Phys. Rev. A* **5**, 1852 (1972).
- [8] A. J. Lichtenberg, M. A. Lieberman, R. H. Cohen, *Physica D: Nonlinear Phenomena* **1**, 291 (1980).
- [9] A. J. Lichtenberg, M. A. Lieberman, *Regular and Chaotic Dynamics*. Appl. Math. Sci. 38, Springer Verlag, New York (1992).
- [10] E. D. Leonel, *J. Phys. A: Math. Theor.* **40**, F1077 (2007).
- [11] B. Batistić, M. Robnik, *J. Phys. A: Math. Theor.* **44**, 365101 (2011).
- [12] G. Papamikos, M. Robnik, *J. Phys. A: Math. Theor.* **44**, 315102 (2011).
- [13] A. B. Ryabov, A. Loskutov, *J. Phys. A: Math. Theor.* **43**, 125104 (2010).
- [14] B. Liebchen, et al., *New Journal of Physics* **13**, 093039 (2011).
- [15] A. K. Karlis, P. K. Papachristou, F. K. Diakonou, V. Constantoudis, and P. Schmelcher, *Phys. Rev. Lett.* **97**, 194102 (2006).
- [16] E. D. Leonel, P. V. E. McClintock and J. K. L. da Silva, *Phys. Rev. Letters*, **93**, 014101 (2004).
- [17] A. C. J. Luo, *ASME J. Vib. Acoust.* **124**, 420 (2002).
- [18] A. C. J. Luo, R. P. S. Han, *Nonlinear Dynamics* **10**, 1 (1996).
- [19] O. F. de Alcantara Bonfim, *Int. J. Bifurcation Chaos* **22**, 1250140 (2012).
- [20] S. Mingalev, D. Lyubimov, T. Lyubimova, *Microgravity Sci. Technol.* **23** (Suppl 1):S99-S103 (2011).
- [21] E. S. Medeiros et al. *Phys. Letters A* **374**, 2628 (2010).
- [22] S. L. T. de Souza, I. L. Caldas, R. L. Viana, *Mathematical Problems in Engineering*, 290356 (2009).
- [23] A. C. J. Luo, Y. Guo, *Mathematical Problems in Engineering*, 298906 (2009).
- [24] A. K. Karlis, et al. *Phys. Rev. E* **78**, 046213 (2008).
- [25] J. de Simoi, D. Dolgopyat, *Chaos* **22**, 026124 (2012)
- [26] Y. Guo, A. C. J. Luo, *J. Of Vibroengineering* **13**, 66 (2011).
- [27] A. C. J. Luo, Y. Guo, *J. Comput. Nonlinear Dynam.* **5**(4), 041007 (2010).
- [28] G. M. Zaslavsky, *Phys. Lett. A* **69**, 145 (1978).
- [29] L. D. Pustynnikov, *Theor. Math. Phys.* **57**, 1035 (1983).
- [30] A. L. P. Livorati, D. G. Ladeira and E. D. Leonel, *Phys. Rev. E* **78**, 056205 (2008).
- [31] B. V. Chirikov, *Phys. Rev.* **52**, 263 (1979).
- [32] M. Ragulskis and M. A. F. Sanjaún, *New J. Phys.* **10**, 083017 (2008).
- [33] M. Mracek and J. Wallaschek, *Mater. Chem. Phys.* **90**, 378 (2005).
- [34] M. S. Talary, J. P. H. Burt, J. A. Tame and R. Pethig, *J. Phys. D: Appl. Phys.* **29**, 2198 (1996).
- [35] D. F. Tavares, E. D. Leonel, *Braz. J. Phys.* **38**, 58 (2008).
- [36] D. F. Tavares, E. D. Leonel, R.N. Costa Filho, *Physica A* **391**, 5366 (2012).
- [37] W. H. Press, B. P. Flannery, S. A. Teukolsky, W. T. Vetterling, *Numerical Recipes in Fortran 77: The Art of Scientific Computing*, Cambridge University Press, Cambridge 1992.
- [38] U. Feudel, C. Grebogi, B. R. Hunt, J. A. Yorke, *Phys. Rev. E* **54**, 71 (1996).
- [39] U. Feudel, C. Grebogi, *Chaos* **7**, 4 (1997).
- [40] D. F. M. Oliveira, E. D. Leonel, *Physics Letters A* **376**, 3630 (2012).
- [41] J. A. C. Gallas, *Phys. Rev. Lett.* **70**, 2714 (1993).
- [42] J. A. C. Gallas, *Appl. Phys. B* **60**, S203 (1994).
- [43] J. A. C. Gallas, *Physica A* **202**, 196 (1994).
- [44] D. F. M. Oliveira, E. D. Leonel, *New J. Phys.* **13**, 123012 (2011).
- [45] D. R. da Costa, C. P. Dettmann and E. D. Leonel, *Phys. Rev. E* **83**, 066211 (2011).
- [46] J. A. de Oliveira, C. P. Dettmann, D. R. da Costa and E. D. Leonel, *Phys. Rev. E* **87**, 062904 (2013).
- [47] J. P. Eckmann, D. Ruelle, *Rev. Mod. Phys.* **57**, 617 (1985).